ADVANCED MATERIALS
www.advmat.d

Analyzing Energy Materials by Cryogenic Electron Microscopy

*Xiao-Chuan Ren, Xue-Qiang Zhang, Rui Xu, Jia-Qi Huang, and Qiang Zhang**

Safe and high-energy-density rechargeable batteries are increasingly indispensable in the pursuit of a wireless and fossil-free society. Advancements in present battery technologies and the investigation of next-generation batteries highly depend on the ever-deepening fundamental understanding and the rational designs of working electrodes, electrolytes, and interfaces. However, accurately analyzing energy materials and interfaces is severely hindered by their intrinsic limitations of air and electron-beam sensitivity, which restrains the research of energy materials in a low-efficiency trial-and-error paradigm. The emergence of cryogenic electron microscopy (cryo-EM) has enabled the nondestructive characterization of air- and electron-beam sensitive energy materials in the microscale and nanoscale, and even at atomic resolutions, affording closer insights into the primary chemistry and physics of working batteries. Herein, the development of cryo-EM and the applications in detecting energy materials are reviewed and analyzed from its overwhelming advantages in disclosing the underlying mystery of energy materials. Critical sample preparation methods as the precondition for cryo-EM are compared, which strongly affect the characterization accuracy. Furthermore, new developments in the analysis of energy materials, especially bulk electrodes and interfaces in lithium metal batteries, are presented according to different functions of cryo-EM. Finally, future directions of cryo-EM for analyzing energy materials are prospected.

1. Introduction

The commercialization of rechargeable lithium-ion (Li-ion) batteries is resulting in a wireless and nonfossil society, which has reshaped our daily lives significantly.[1] Currently, the rapid developments of portable and wearable electronics, electrical vehicles, and smart grids are necessitating safer and more high-energy-density secondary batteries.[2] Moreover, the storage and transportation of increasing renewable and clean energy, which is intermittently generated at remote areas, require more inexpensive rechargeable battery systems.[3] Safe, high-energy-density, and low-cost next-generation rechargeable batteries are in strong pursuit.[4] Nevertheless, the specific energy of state-of-the-art commercial Li-ion batteries cannot satisfy the increasing demand owing to the limited theoretical specific energy.[5] The theoretical specific energy of present Li-ion batteries is approximately 350 Wh kg^{-1} based on a 18 650 cell configuration, in which graphite is employed as anode and transition metal oxides as cathode.[6] To achieve a higher specific energy, next-generation batteries based on different energy chemistries have been proposed, among which Li metal batteries are reviving and attracting significant attention from both academia and industry.[7] Undoubtedly, innovations and breakthroughs in Li metal batteries with higher specific energies rely on the comprehensive understanding of the operating principles and failure mechanisms of working batteries, which ensure the rational design of energy materials and accelerate the pace of research and development.[8]

Generally, energy materials, such as electrodes, electrolytes, and interfaces, are highly reactive and sensitive to air and electron beam, especially after repeated cycling. This prevents us from accurately acquiring their credible structure, chemical information, and evolution behavior, resulting in a low-efficiency trial-and-error research paradigm.[9] Li metal is intrinsically highly reactive, and the characterization of Li metal is challenging.[10] When it is exposed to air at room temperature, especially moist air, the surface of Li metal is covered with Li_2O, Li_3N, and Li_2CO_3, passivating the original fresh Li surface and interfering with the assessment of results.[9a,11] When it is exposed to high-energy electron beams at room temperature, Li metal transmutes owing to its low melting point; therefore, it cannot preserve its original structure.[12] Owing to its high reactivity, Li metal can react with electrolytes to obtain a solid electrolyte interphase (SEI) in a working battery.[13] The homogeneity of an SEI directly dictates the uniformity of deposited Li and hence the Coulombic efficiency and safety of batteries.[14] An SEI forms on the surface of anode materials operating at low potentials and significantly affects the performance of batteries.[15] However,

---

Dr. X.-C. Ren, X.-Q. Zhang, Prof. Q. Zhang
Beijing Key Laboratory of Green Chemical Reaction Engineering and Technology
Department of Chemical Engineering
Tsinghua University
Beijing 100084, China
E-mail: zhang-qiang@mails.tsinghua.edu.cn
R. Xu, Prof. J.-Q. Huang
Advanced Research Institute for Multidisciplinary Science
Beijing Institute of Technology
Beijing 100081, China

The ORCID identification number(s) for the author(s) of this article can be found under https://doi.org/10.1002/adma.201908293.

DOI: 10.1002/adma.201908293

an SEI is in a metastable state and sensitive to the surrounding, such as air and electron beams. The formation and evolution of SEIs are still unclear owing to challenges in characterization, thereby hindering the rational design of present Li-ion batteries and next-generation Li metal batteries.[15a,16] Similarly, the cathode electrolyte interphase (CEI) is essential but impressionable.[17] Therefore, it is indispensable to collect the intrinsic information of energy materials while preserving the original state in the absence of contamination or destruction.

Cryogenic electron microscopy (cryo-EM) was initially established by Glaeser and Taylor in 1974[18] and credited by the 2017 Nobel Prize in Chemistry. Cryo-EM is a well-established characterization technique in biological sciences for investigating the structure of biological materials.[19] The original morphology and structure of biomaterials can be well preserved at cryogenic temperatures. Inspired by the successful utilization of cryo-EM in biological sciences, researchers have extended its applications to investigate other beam and air-sensitive materials, such as polymers[20] and nanomaterials.[21] Cryo-EM not only inhibits the damage of sensitive materials from air and electron beams during sample transfer and characterization, but also preserves their intrinsic structures, which enables us to image them at the micro/nano/atomic scale.[22] Recently, cryo-EM has been introduced to analyze energy materials.[23] Owing to the prominent advantages of cryo-EM, air-reactive, and beam-intolerant electrodes and the corresponding post-reaction components, such as Li metal, SEI, CEI, and other energy materials, have been widely investigated in recent years (**Figure 1**). Cryo-EM is a powerful tool to disclose the underlying mechanism of energy materials and provide guidance for the rational design of next-generation batteries.

Herein, we first describe the critical sample preparation method as the precondition for cryo-EM, which strongly dictates the accuracy of cryo-EM characterizations. The recent progresses in analyzing energy materials, especially bulk electrodes and interfaces in Li metal batteries, are presented in terms of different functions of cryo-EM. Finally, the future directions of cryo-EM in analyzing energy materials are proposed.

2. Sample Preparation and Transfer for Cryo-EM

Generally, both cryo-focused ion beam (cryo-FIB) and cryogenic transmission electron microscopy (cryo-TEM) can be used to characterize energy materials at cryogenic temperatures according to the resolution demand. For instance, the cross-sectional image of deposited Li can be recorded to evaluate its internal information at the microscale by cryo-FIB and characterize the fine structures of SEI and crystalline Li at the nanoscale by cryo-TEM. The sample preparation methods and transfer processes are crucial as the preceding processes before sample characterization. Appropriate methods can avoid direct contacts between samples with air or heat to obtain pristine information.[24] Three main methods are summarized as follows.

2.1. Bulk Materials at Microscale

To assess the density of deposited bulk Li, thickness of dead Li, and artificial coating on bulk Li, cross-sectional images with microscale resolution is required. Cross-sectional images of deposited bulk Li on Cu foil obtained by cutting with a knife are primarily recorded in standard SEM at room temperature, during which the original morphology is destroyed. Cryo-FIB can cut the bulk Li metal anode and expose its fresh section by high-energy gallium (Ga) ion flux milling and simultaneously probe the morphology by secondary electron or backscatter electron imaging at the microscale (**Figure 2**a). The sample placed in a cryo-FIB system is in thermal contact with a cryo-stage under continuous chilled nitrogen gas cooling and remains

Xiao-Chuan Ren received his Ph.D. degree in optical engineering from Wuhan National Laboratory for Optoelectronics at Huazhong University of Science and Technology. He is currently a postdoctoral researcher in Prof. Qiang Zhang's group at the Department of Chemical Engineering in Tsinghua University. His present research interests focus on functional materials and their advanced characterizations for next generation batteries.

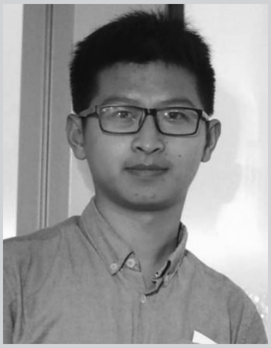

Xue-Qiang Zhang obtained his bachelor's at Tianjin University in 2016. He is currently a Ph.D. candidate at the Department of Chemical Engineering, Tsinghua University with Prof. Qiang Zhang. His research interests focus on Li metal batteries, especially Li metal anodes and interfaces between Li and electrolyte.

Qiang Zhang received his bachelor's and Ph.D. degree from Tsinghua University in 2004 and 2009, respectively. After a stay in Case Western Reserve University, USA, and Fritz Haber Institute of the Max Planck Society, Germany, he was appointed as an associate professor in Tsinghua University in 2011. He was promoted to a full professor in 2017. His current interests focus on energy materials, includes Li–S batteries, Li metal anodes, and electrocatalysts.

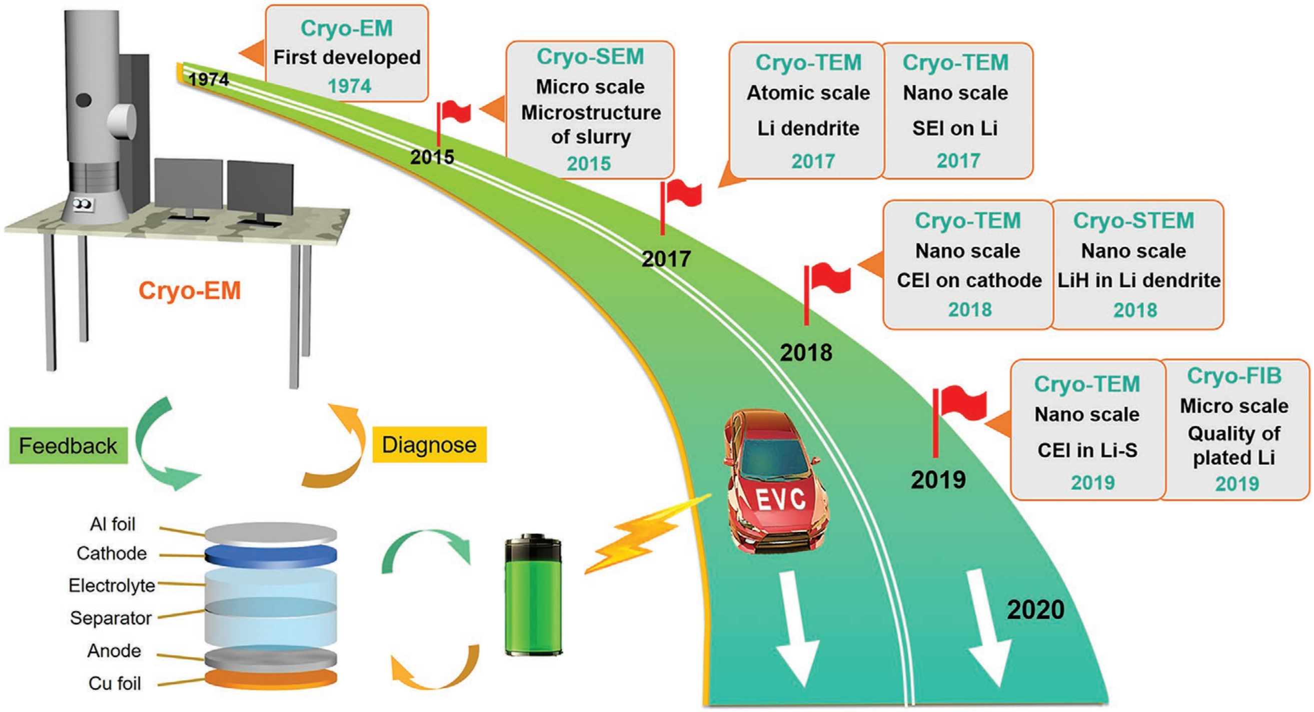

Figure 1. The summary of cryo-EM in analyzing energy materials in a historical scope. Cryo-EM (cryo-TEM) was initially developed in 1974[18] and first applied to analyze energy materials (Li[12] metal and SEI[12,22a]) until 2017. The CEI on transition metal oxide cathode was captured and identified by cryo-TEM in 2018[53] and in the same year, LiH was confirmed as a type of Li dendrite via cryo-STEM.[28a] After that, the CEI in Li–S batteries was characterized by cryo-TEM in 2019.[54] Cryo-SEM/FIB was also employed to characterize the energy materials in recent years, such as the battery slurry[60] and Li metal anode[61] in 2015 and 2019, respectively. The significant discoveries of cryo-EM in analyzing energy materials are mushrooming and great breakthroughs in the development of battery will come by the accurate diagnosis and feedback of cryo-EM.

at a stable cryogenic temperature for several hours.[25] Therefore, the pristine state of the sample features can be preserved after ion milling. On the contrary, routine FIB used to cut Li metal induces deleterious morphological modifications of Li at room temperature during milling owing to the low melting point, large thermal conductivity, and low shear modulus of Li. Additionally, the ion damage of energy materials, such as ion implantation, lattice damage, and crystal transformation stemmed from Ga ion milling is serious at room temperature.

2.2. Bulk Materials at Nanoscale

Cryo-TEM can capture high-resolution images less than 0.3 nm. However, it is still a challenging to prepare air or heat-sensitive bulk samples with a small size (<100 nm) on a contamination-free TEM grid.[6a,26] Cryo-FIB is a powerful tool for trimming bulk materials to a slice that is then mounted onto a TEM grid (Figure 2b).[27] Cryo-FIB, benefitting from the low-temperature surrounding as above stated, can curtail the bulk samples to the required size by Ga ion milling without beam damage. Subsequently, the as-obtained slice with well-maintained interfaces between the electrode material and liquid electrolyte can be installed on a transfer holder and further transferred to cryo-TEM for characterization.[28] However, it will suffer inevitable air access during the vacuum chamber pressure loss of cryo-FIB when transferring grids from cryo-FIB to cryo-TEM, which inextricably affects the components, contents, and even SEI thickness, such as through the formation of $LiCO_3$, Li_2O, and LiH, which interferes the characterization accuracy.

2.3. Nanomaterials at Nanoscale

Except the slice milling and transfer method by cryo-FIB, mounting air-sensitive nanomaterials to a TEM grid without artifacts is difficult. The developed in situ growth of energy materials (such as Li[22a] and Si[29]) on a TEM grid is a practical approach to alleviate the damage or contamination of samples and maintain their intrinsic nature compared with other multistep fabrication and transfer processes.[30] For instance, Li metal can be directly deposited on a TEM grid in a coin cell (Figure 2c). The grid is removed from a cell and sealed in a glovebox. Subsequently, the grid is transferred to a TEM room for installation on a TEM transfer holder. Two types of transfer holders exist, including cryo and cooling holders.[12,22a] When using a cryo transfer holder, the TEM grid installation process should be operated in liquid nitrogen (N_2) such that the sample remains frozen and to reduce the sample reactivity. The grid can be sealed in an Eppendorf tube, which can be conveniently transferred and plunged into a bath of liquid N_2 and easily crashed for quick exposure at cryogenic temperatures without direct contact with air.[12] The morphology of the deposited Li and the as-formed SEI on the Li surface after cycling can be detected. However, some loose deposited Li and unstable surface SEIs can dissolve into liquid N_2 at the frozen specimen

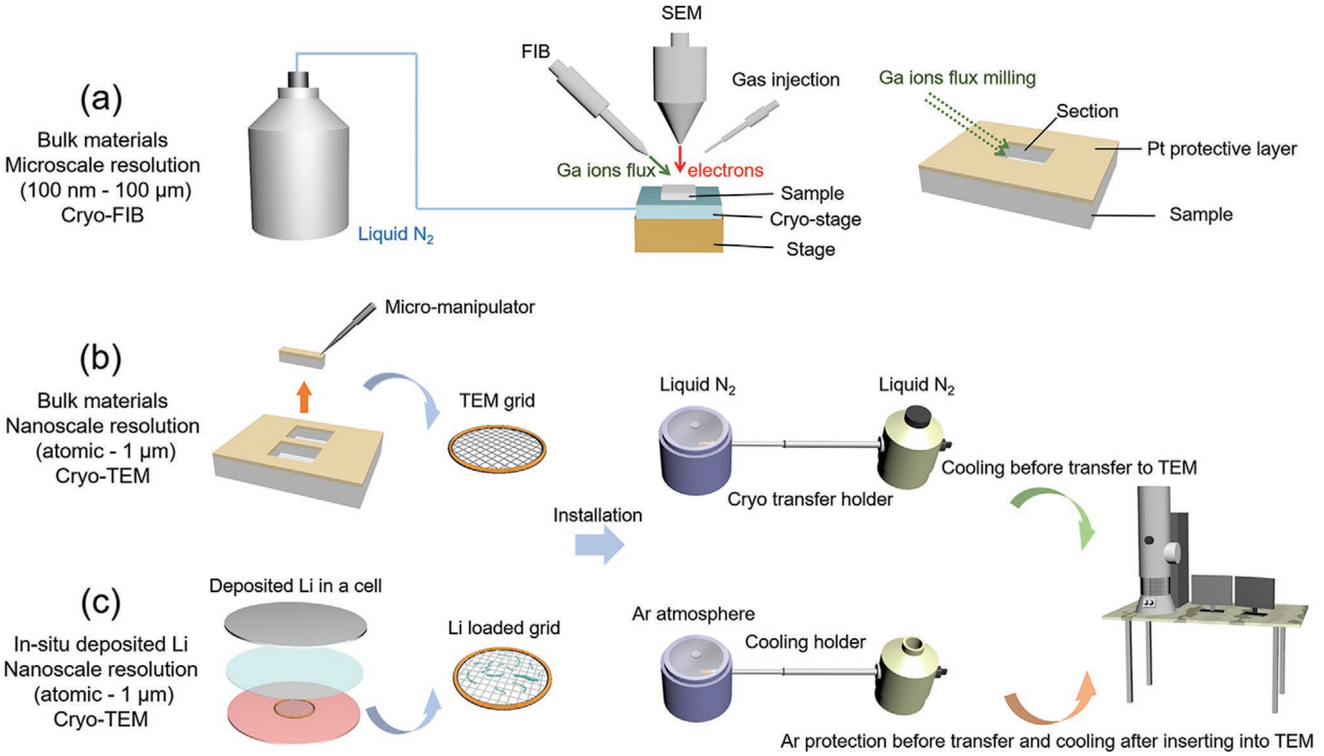

Figure 2. Schematic of the processes of sample preparation for cryo-EM. a) The cross-sectional area of bulk energy material was obtained by Ga ions milling and characterized in cryo-FIB at microscale. b) Trimming the bulk material into a thin slice by cryo-FIB and transferring it to cryo-TEM for a nanoscale characterization. c) The nanomaterial obtained by in situ deposition or growth in TEM grid and captured at nanoscale by cryo-TEM. The cryo transfer holder should be cooled by liquid N_2 previously and the grid is sealed with a closed shuttle before transferring into TEM. While using the cooling holder, the grid is protected by Ar without liquid N_2.

stage, which interferes the accuracy of the experimental results. Moreover, crystalline water generates inevitably when the sample is in contact with liquid N_2, and it will be introduced during grid transfer processes. Operating a cooling holder is easy, and the sample is cooled down immediately after the holder is inserted into the TEM chamber. It is noteworthy that both sample installation and transfer processes should be protected in an argon (Ar) atmosphere in a glovebox, glovebag, or other Ar-filled containers.[22a,30] The cooling holder can avoid the ingress of air and liquid N_2 is protected on the sample. This reduces the potential damage of the Li metal and other sensitive components on the electrode. These two types of holders have been proven to possess good practicability. However, a holder that can concurrently avoid sample exposure to air and achieve rapid cooling should be focused in further research and development, which is expected to simplify the operation procedures and achieve nondestructive transfer processes.

3. High-Resolution Characterization by Cryo-TEM

TEM has been widely applied to investigate energy materials.[31] Crystal and amorphous components and their corresponding distributions can be identified based on image contrasting, crystalline lattice spacing, selected area electron diffraction (SAED), and fast Fourier transform (FFT) coupled with TEM. Combining the advantages above and cryogenic conditions, cryo-TEM can be used to capture the crystalline structure of Li dendrites and the composition information of SEI at nano and atomic scale resolutions.

3.1. Atomic Resolution of Li Metal Dendrites

It is important to investigate the intrinsic growth behavior of Li metal, which exhibits a direct correlation with the cycling efficiency and stability of a working battery. Li metal is highly reactive at room temperature. During sample transfer, Li suffers from corrosion by water and oxygen upon brief air exposure.[32] In addition, weak atomic bonding and low melting point cause Li metal to be extremely unstable under electron beams.[33] Cui and co-workers demonstrated that the air-exposed Li dendrites exhibited polycrystalline artifacts in standard TEM, and burned holes appeared after a transitory exposure to electron beams (**Figure 3**a).[34] Li dendrites can preserve their original structural and chemical information at cryogenic temperatures owing to the low reactivity between Li metal and liquid N_2 and suppressed heat accumulation under electron beam irradiation. Therefore, it is possible to directly visualize Li metal with an atomic resolution of 0.7 Å by spherical-aberration-corrected TEM at cryogenic temperatures. The atomic-resolution observation of Li metal was achieved (Figure 3b) and the growth direction of Li dendrites in carbonate-based electrolytes (ethylene carbonate/diethyl carbonate, EC/DEC) was identified

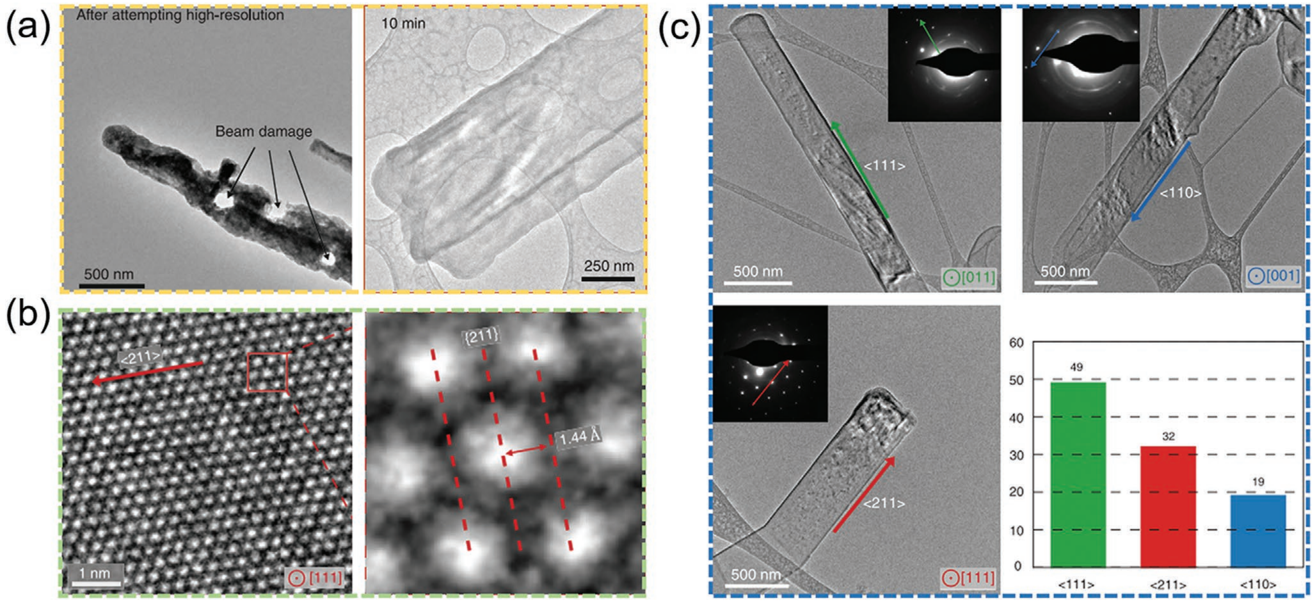

Figure 3. a) TEM images of Li dendrites after exposure to electron dose rate of ≈500 e Å^{-2} s^{-1} for ≈1 s at room temperature and after continuous electron-beam irradiation of 10 min at a dose rate of ≈50 e Å^{-2} s^{-1}. b) Atomic-resolution cryo-TEM images of Li metal. c) The cryo-TEM images, corresponding SAED pattern of Li dendrites, and their statistic preferred growth directions. a–c) Reproduced with permission.[12] Copyright 2017, The Authors, published by AAAS.

(Figure 3c).[12] The cryo-TEM images of Li dendrites show a lighter contrast than standard TEM images owing to the single crystal feature of deposited Li dendrites. The nanowires of Li dendrites exhibited a body-centered cubic crystal structure and grew along three primary directions of <111>, <110>, and <211> in EC/DEC electrolyte to reduce the surface energy by exposure the most densely packed {110} planes (Figure 3c).

3.2. Chemistries of SEI

The SEI located on the surface of the anode exhibits electron-insulative and ionic-conductive properties, which are generated by reactions between the electrolyte and Li metal. The SEI on the Li metal anode plays an indispensable role in dictating the Li plating pattern. However, information regarding the SEI component in batteries is insufficient.[35] The structure and composition of the SEI strongly relies on the formulation of electrolytes, including solvents, Li salts, and additives.[36] However, owing to the air- and beam-sensitive features, it is challenging to capture the original morphology, composition, and chemical distributions of the SEI through routine characterizations.[37] Therefore, cryo-TEM is applied to mitigate the problems above.

The presence of fluoroethylene carbonate (FEC) additives in an EC/DEC electrolyte can significantly improve the cycling performance of a Li metal anode.[38] Cui and co-workers employed cryo-TEM to investigate the structure and composition of SEIs formed in different electrolytes to disclose the role of FEC additives.[12] The SEI generated in standard EC/DEC electrolytes is composed of small inorganic crystalline domains (Li_2O and Li_2CO_3) randomly embedded into amorphous organic polymer matrices, which is called a mosaic nanostructure (**Figure 4**a).[39] However, when FEC additives are added, an ordered SEI nanostructure with a bilayer nanostructure containing an inner amorphous polymer matrix and an outer inorganic layer (Li_2O, Li_2CO_3 and possible LiF) is confirmed, as evident through cryo-TEM images. The bilayer nanostructure is consistent with the multilayer SEI structure proposed by Aurbach and co-workers.[40] However, the orders of inorganic and organic layers are opposite. It is widely accepted that the presence of LiF in SEIs formed by FEC additives is important for the performance improvement of Li metal anodes owing to its high surface energy and stability. Meng et al. captured the presence of crystalline LiF in the SEI of Li metal anodes based on cryo-TEM.[22a] FFT pattern revealed two clear and bright spots with 0.2 nm lattice spacing in the SEI region, which is consistent with the lattice distance of LiF (200) (Figure 4b). Moreover, the fine structure of the F K-edge obtained from electron energy loss spectroscopy (EELS) under the freezing condition further confirmed the contribution of LiF in the SEI.

Cryo-TEM affords a reliable visual evidence regarding the formation of distinct structures of SEIs with FEC additives in carbonate-based electrolytes. The ordered bilayer SEI nanostructure can offer enhanced mechanical durability than normal mosaic SEIs, rendering it more effective in passivating Li metal and hence improved cycling performances and high Coulombic efficiency (CE) in cells.[12] Recently, Cui and co-workers demonstrated that a bilayer SEI nanostructure can be generated on Li metal anodes by adding lithium nitrate ($LiNO_3$) additives in carbonate-based electrolytes (EC/DEC), as confirmed through cryo-TEM.[41] The bilayer SEI comprised highly ordered crystalline Li_2O in the outer layer and an amorphous matrix in the inner layer with scattered Li_2O and Li_2CO_3 (**Figure 5**a). Despite similar bilayer SEI films on the surface of the Li metal anode, the nucleation of Li changes from dendritic to spherical by the elaborate detection of cryo-TEM when changing the additives from FEC to $LiNO_3$ in carbonate-based electrolytes. The intrinsic

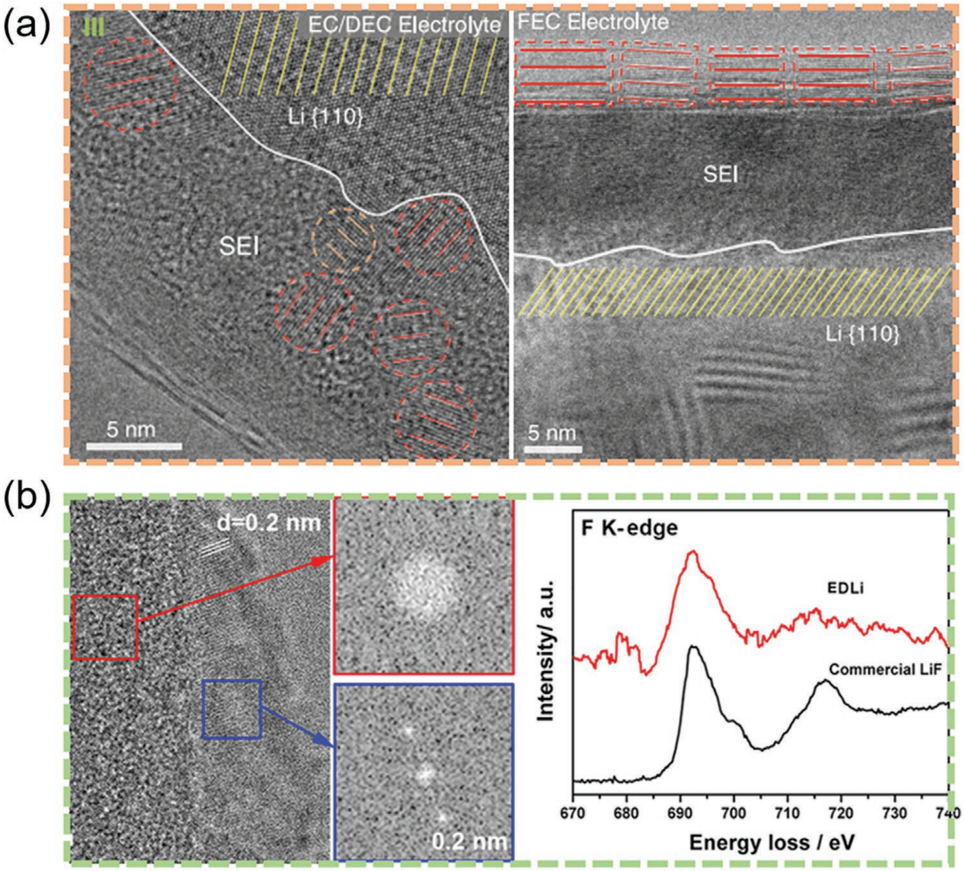

Figure 4. a) High-resolution TEM images of the SEI on the surface of Li metal in standard electrolyte and the electrolyte with FEC additives. Reproduced with permission.[12] Copyright 2017, The Authors, published by AAAS. b) Cryo-TEM images with FFT pattern and EELS spectra of deposited Li formed in EC/DEC electrolyte. Reproduced with permission.[22a] Copyright 2017, American Chemical Society.

difference of Li deposition morphology closely depends on the physicochemical properties of the SEI, such as ion transport kinetics and interfacial energy, which should be further investigated according to the results of cryo-TEM. The formation of spherical morphology of the deposited Li metal also occurred in the electrolyte of 1.0 M lithium bis(trifluoromethanesulphonyl) imide (LiTFSI) dissolved in 1,3-dioxolane/1,2-dimethoxyethane (DOL/DME) as a solvent with 1% $LiNO_3$ additive. Furthermore, the size of the deposited Li particles and the corresponding SEI nanostructures are closely dependent on temperature, as revealed by cryo-TEM.[42] The formed deposited Li particles at high temperatures are larger than those at room temperature owing to the faster charge transfer and smaller overpotential at elevated temperatures. Additionally, a thicker and inverse-layered SEI formed at high temperatures, which differ significantly from the amorphous SEI generated at room temperature. Furthermore, the types and concentration of electrolytes affected the formation of the bilayer SEI. When a high concentration electrolyte of 10 M lithium bis(fluorosulfonyl) imide (LiFSI) in dimethyl carbonate (DMC) was used, the surface of a wrinkled graphene cage matrix can form the ordered bilayer SEI after Li deposition (Figure 5b).[43] The SEI is composed of a Li_2O-rich outer layer and a polymerized inner layer, which is similar to the SEI formed in 1.0 M lithium hexafluorophosphate ($LiPF_6$) with EC/DEC solvent and FEC additives. The cryo-TEM images reveal a much thinner SEI owing to the decreased reactive reduction of FSI^- anions around the surface of graphene in high concentrations instead of that of DMC solvents. Consequently, the cycling performance of a battery is better than that in $LiPF_6$ with EC/DEC solvent and 10% FEC as well as 1% vinylene carbonate (VC) additives. However, the formation mechanism of the ordered bilayer SEI in electrolyte remains vague. Therefore, more studies are necessitated to resolve the different SEI structures formed through various energy chemistries in operating electrolytes.

3.3. Correlation between Li Utilization and SEI Chemistries

The structure and composition of the SEI are highly dependent on the stripping process of the deposited Li, which consequently dictates the utilization efficiency of the Li metal anode. An SEI with different distributions of crystalline grains can regulate the ion transport behavior in special regions along the dendrites, which is attributed to space-charge effects[44] or the affinity between the functional groups on the surface of the SEI and the solvents and anions in the electrolyte;[45] this further determines the uniformity of Li stripping. The role of an SEI nanostructure in Li stripping has been recently reported by Li et al[46] Cryo-TEM was employed to characterize the functions

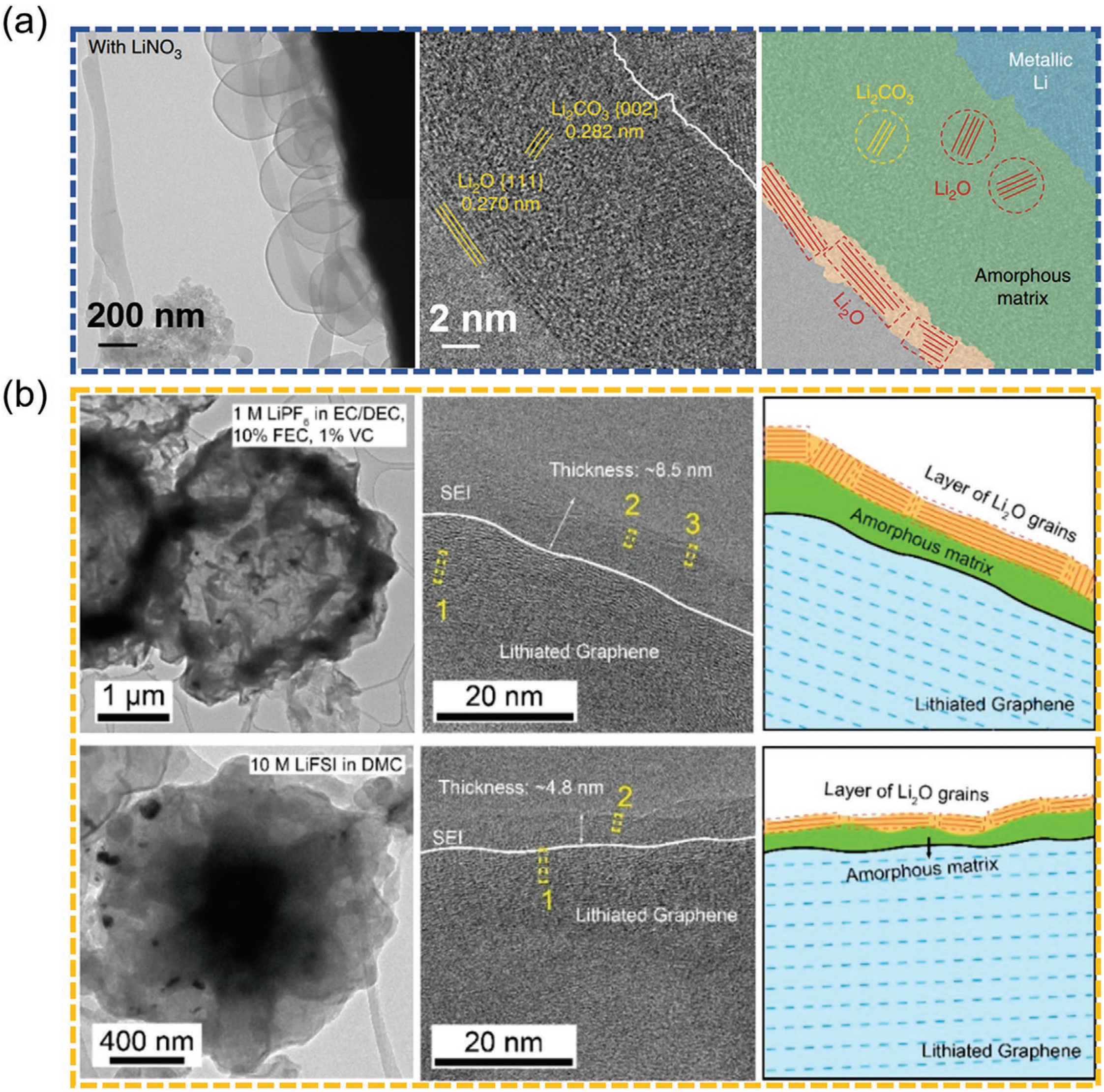

Figure 5. a) Cryo-TEM images and the corresponding schematics of SEI structure formed on the surface of Li metal in EC/DEC electrolyte with $LiNO_3$ additives. Reproduced under the terms of the CC-BY Creative Commons Attribution 4.0 International license (http://creativecommons.org/licenses/by/4.0/).[41] Copyright 2018, the Authors, Published by Springer Nature. b) Cryo-TEM images of the wrinkled graphene cages and the corresponding schematics of SEI after Li metal deposition using the electrolyte of 1 M $LiPF_6$ in EC/DEC with 10% FEC and 1% VC additives, and 10 M LiFSI in DMC without any additives. Reproduced with permission.[43] Copyright 2019, American Chemical Society.

of two distinct SEIs (bilayer and mosaic structures), and their nanostructures were correlated with the performances of Li metal batteries (**Figure 6**a). The mosaic nanostructured SEI composed of nanocrystalline components of Li_2O and Li_2CO_3 with higher ionic conductivity but nonuniform distribution can form notches on the surface of the stripped dendrites at high concentration regions. The notches can completely evolve into cleavages as the nonuniform stripping process continues, resulting in an electronic disconnection of partial Li metal in the dendrites, which can be clearly captured by cryo-TEM. By contrast, a bilayer nanostructured SEI with a uniform crystalline grain concentration in any region can promote a complete stripping of Li along the dendrites, resulting in less dead Li generation. In addition, Meng and co-workers described that the content of inactive (dead) Li may depend on the morphology of deposited Li or Li dendrites.[47] Cryo-TEM images showed that the formed whisker morphology of deposited Li with large tortuosity in a practical carbonate electrolyte (CCE) exhibited a high content of dead Li, resulting in a low first-cycle CE. The inactive Li formed in CCE after stripping was isolated by the surrounding SEI and retained a whisker-like morphology (Figure 6b). However, dense Li with a chunky morphology and a low tortuosity content of metallic Li in a high-concentration electrolyte (HCE) maintained the structural connection and intimate contacts with the current collectors, resulting in little dead Li reservation and a high CE.

Chueh and co-workers employed cryo-TEM to investigate the evolution of a mosaic SEI formed on a carbon black anode during cycling to provide visual evidence for the effect of a general mosaic-nanostructured SEI on battery cycling performance in EC/DEC electrolyte (**Figure 7**a).[48] The amorphous SEI can form on carbon black after one cycle. However, two

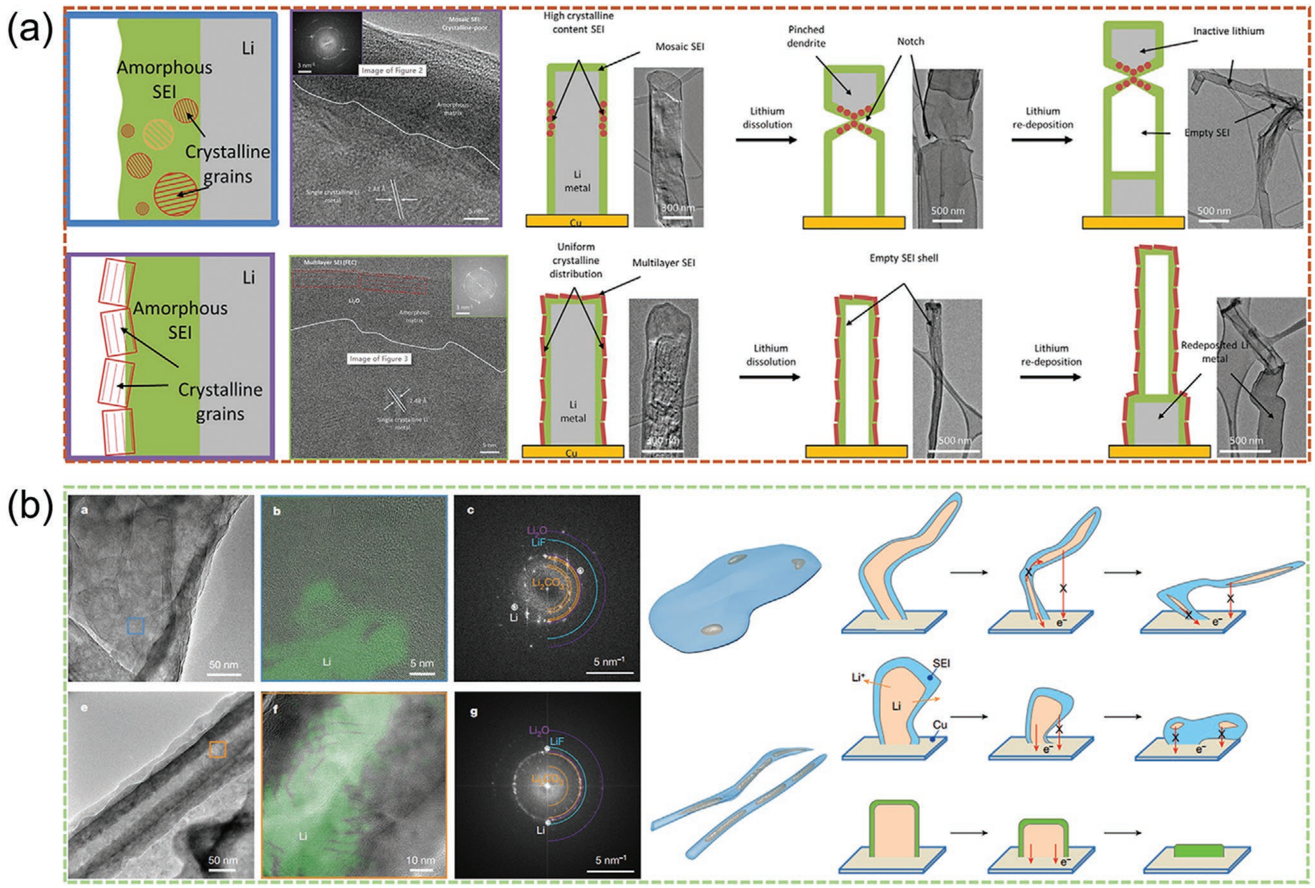

Figure 6. a) Cryo-TEM images and schematics of the typical formation of a Li metal dendrite, stripping and redeposited in EC/DEC electrolyte and EC/DEC electrolyte with 10 vol% FEC additives. Reproduced with permission.[46] Copyright 2018, Elsevier. b) Cryo-TEM images and schematics of the formed residual dead Li after stripping process in different electrolytes. Reproduced with permission.[47] Copyright 2019, Springer Nature.

vastly contrasting morphologies of SEIs generated on separate carbon black nanoparticles after 20 cycles, including a compact SEI of thickness 5 nm and an extended SEI layer of ≈100 nm. The compact SEI comprised inorganic components (Li_2O, LiOH, and Li_2CO_3) distributed in an amorphous matrix to form the mosaic-structured SEI, while the extended SEI contained no crystalline component and spanned a much large length scale, binding among many electrode particles. The extended SEI can reduce the electrode porosity and increase the overpotential for the ion transportation; however, it exhibits poor passivation, owing to the lack of low-conductive and high dielectric crystalline components.[49] The SEI nanostructure evolving over the voltage change on the electrode materials is critical. Cui and co-workers recently observed the voltage-dependent, stepwise evolution of an SEI nanostructure on CuO nanowires during the initial charge of batteries through cryo-TEM.[50] The thickness of the SEI increased continuously during discharge in EC/DEC electrolyte with FEC additives, accompanied with crystalline grains of Li_2O/Li_2CO_3 nucleating at 0.5 V and the formation of a bilayer nanostructured SEI at 0 V (Figure 7b). When the potential was further reduced to below 0 V, the deposited Li exhibited a much thicker SEI with a significant growth in the amorphous component, indicating the continuous electrochemical decomposition of the electrolyte under the overpotential of Li deposition. This illustrated that the bilayer nanostructured SEI formed in the carbonate-based electrolyte was penetrable to the electrolyte. Therefore, although a significantly improved cycling performance was achieved in the carbonate-based electrolyte with FEC additives, partial capacity attenuation appeared. Cryo-TEM enabled the unambiguous observation of the structure and chemical components of the SEI at various discharged voltages, highlighting the necessity for a well passivated and effective SEI.

3.4. Artificial SEI Layer

Recently, artificial SEI layers have been widely investigated owing to their ability to inhibit the growth of Li dendrites and further improve the cycling performance of Li metal batteries. Many coating strategies, such as gas phase reaction, solution processes, or atomic layer deposition have been introduced to generate an artificial layer on the surface of Li, which yielded significant improvement in battery performance.[51] Recently, Meng and co-workers described a lithium methyl carbonate (LMC) coating layer on the surface of Cu and achieved enhanced Li deposition performance in the electrolyte of lithium iodide dissolved in EC/DMC mixed

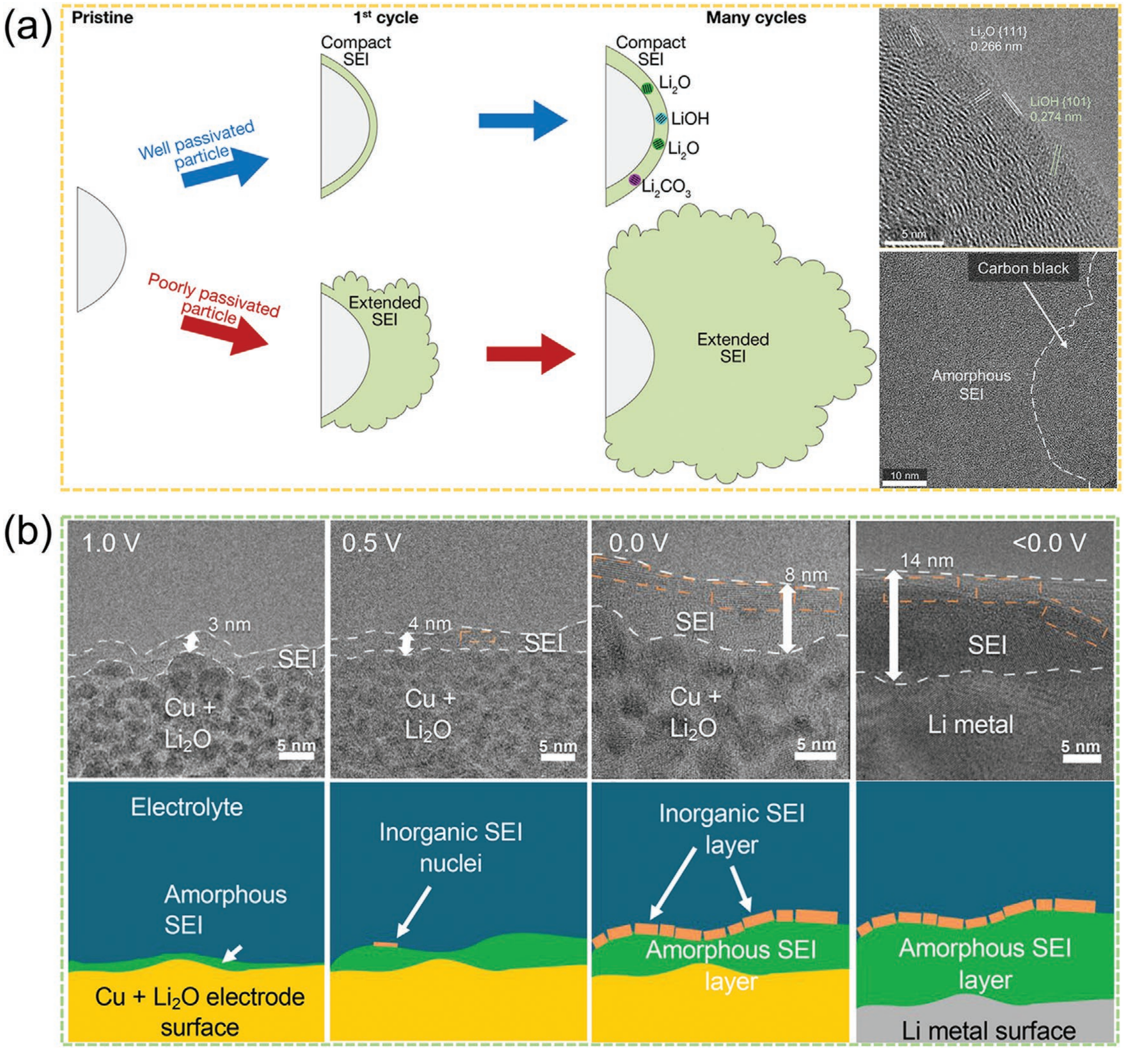

Figure 7. a) Schematics and cryo-TEM images of different types of SEI formed on the surface of carbon black anode after cycling. Reproduced with permission.[48] Copyright 2019, American Chemical Society. b) Cryo-TEM images and illustrations of the structural evolution of the SEI nanostructure formed on CuO at different potentials and Li metal deposition in EC/DEC with 10% FEC additives. Reproduced with permission.[50] Copyright 2019, American Chemical Society.

solvents. Cryo-TEM proved that LMC is the only chemical species coating on Li, promoting an agglomerated Li deposition rather than dendritic Li (**Figure 8**a).[30] Wang and coworkers synthesized an artificial molecular-level SEI derived by a reactive polymer composite (RPC) as SEI precursors.[52] The special SEI nanostructure with excellent passivation properties, homogeneity, and mechanical strength effectively suppressed electrolyte consumption. Cryo-TEM displayed three layers recognized: unreacted RPC, RPC-derived SEI, and Li. The RPC-derived SEI was composed of major amorphous polymeric Li salt components with GO nanosheets and LiF nanoparticles. This artificially homogeneous and dense SEI nanostructure shown from cryo-TEM images differed from the routine electrolyte-derived SEI with multilayered or porous nanostructure, which contributed to the effective suppression of Li dendrite growth and enhanced SEI stability.

3.5. Cathode Electrolyte Interphase

The cathodes in Li-ion battery present interfacial problems owing to the formation of the CEI by electrolyte oxidation at high voltages. The nanostructure and composition of the CEI affects the cycling performance and the CE of cathodes. Cryo-TEM is important for the accurate measurement of the pristine structure of the CEI and reveals the relevance between the CEI and cathode performance. Recently, Xu and co-workers investigated a carbonate-free electrolyte system based on a single sulfone solvent combined with LiFSI to achieve a high-voltage cathode ($LiNi_{0.5}Mn_{1.5}O_4$).[53] Cryo-TEM confirmed that the structure of the CEI formed in the carbonate-based electrolyte exhibited significant variations in thickness and uniformity with open sections of minimal coverage, resulting in a significantly thick CEI and a partially direct exposure of a $LiNi_{0.5}Mn_{1.5}O_4$ surface to the electrolyte (Figure 8b). Conversely,

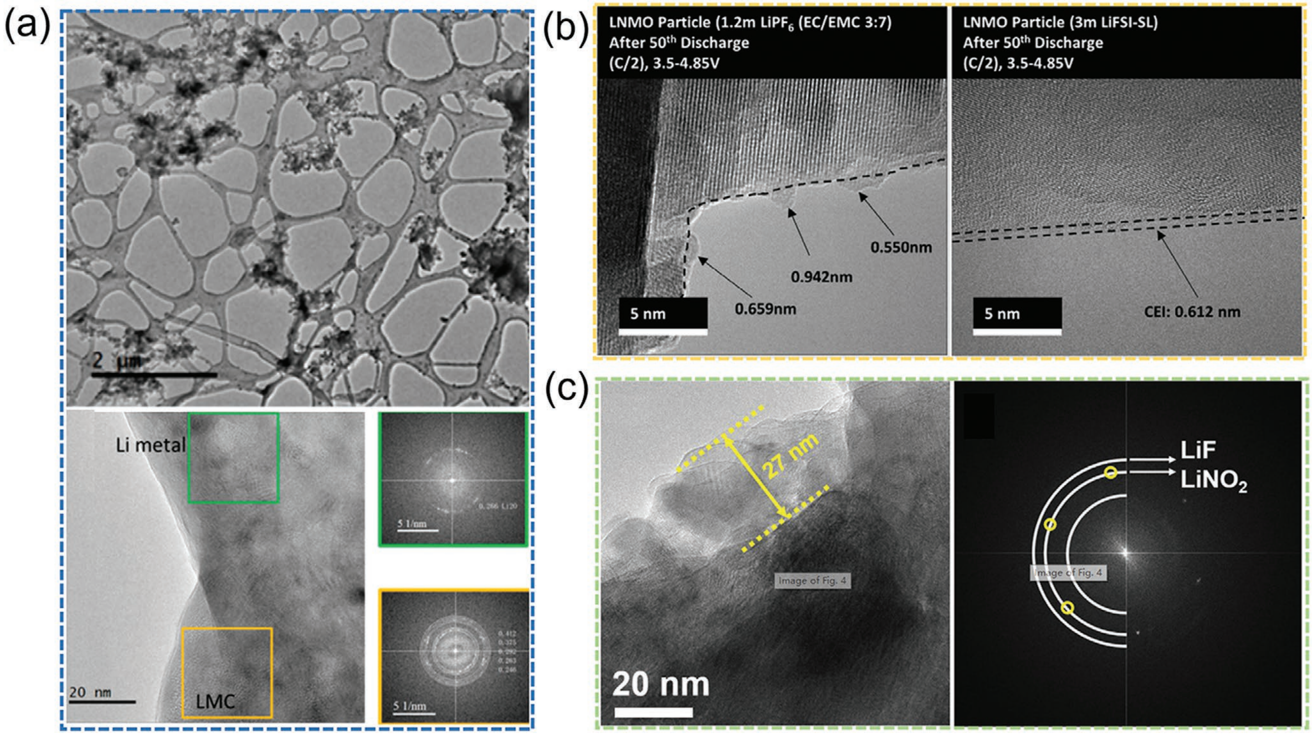

Figure 8. a) Cryo-TEM images and corresponding FFT patterns of CH_3OCO_2Li coating protection layer on the surface of Cu after Li plating. Reproduced with permission.[30] Copyright 2018, American Chemical Society. b) The cryo-TEM images of CEI on $LiNi_{0.5}Mn_{1.5}O_4$ particle after 50 cycles using $LiPF_6$-EC/EMC and LiFSI-sulfone electrolytes. Reproduced with permission.[53] Copyright 2018, Elsevier. c) The cryo-TEM image and corresponding SAED image of SPAN as cathode in Li–S batteries covered with a CEI layer. Reproduced with permission.[54] Copyright 2019, Elsevier.

the CEI formed on $LiNi_{0.5}Mn_{1.5}O_4$ particles in LiFSI-sulfone electrolyte appeared much more uniform in thickness and conformal in surface coverage, which provided strong evidence of improved performance toward the high interfacial stability of new LiFSI-sulfone electrolytes. Liu and co-workers discovered that the sulfurized polyacrylonitrile (SPAN) cathode in Li–S battery could form a CEI on the surface in a high-concentration ether-based electrolyte with LiTFSI and $LiNO_3$ as co-salts.[54] A crystalline CEI of SPAN with LiF and $LiNO_2$ was first observed by cryo-TEM (Figure 8c), explaining the stable cycling of SPAN in ether-based electrolytes derived by the protection of crystalline CEI to avoid the exposure of discharge products of SPAN to large amounts of electrolyte and suppress the formation of soluble polysulfide species.

4. Component Analysis by Cryo-STEM with X-Ray Energy Dispersive Spectroscopy and EELS

Cryo-TEM is a powerful technique to investigate the structure and chemical composition of SEIs formed on the surface of electrode materials. However, the high-resolution of elemental variety, distribution, and quantitative analysis of the SEI and some sensitive electrode materials are difficult to determine through cryo-TEM. Cryo-scanning transmission electron microscopy (cryo-STEM) coupled with X-ray energy dispersive spectroscopy (XEDS) or EELS can overcome these issues. STEM can be used to collect high-resolution Z-contrast images and synchronously capture XEDS or EELS information for every pixel. The morphology and elemental composition information of samples are obtained for each pixel. Moreover, cryo-STEM using low accelerating voltages can further reduce the damage of samples from electron beams as well as deliver improved image contrasts through a high-angle detector.[55] Compared with other element analysis methods, such as X-ray photoelectron spectroscopy, cryo-STEM coupled with XEDS or EELS can accurately characterize the chemical composition and distribution information of air- and temperature-sensitive materials under frozen conditions, avoiding potential destruction of samples by direct air exposure at room temperature during transfer processes.

Recently, Kourkoutis and co-workers identified that two types of Li dendrites coexisted on a Li anode in EC/DMC electrolyte through cryo-STEM and EELS.[28a] By investigating the chemical mapping of solid–liquid interfaces, two types of dendrites with distinct structures and compositions were captured. The cryo-STEM images and EELS mapping revealed an extended SEI (300–500 nm thick) with increased concentration of oxygen and Li compared with the electrolyte, and no fluorine appeared on the surface of type I dendrites (**Figure 9**a), while type II SEI exhibited thin, carbon-free, lithium and oxygen-rich coating layers. LiH appeared in almost all parts of type II dendrites, but small LiH regions appeared on type I dendrites. Insights into the formation of different types of Li dendrites from cryo-STEM provide emerging understanding of solid–liquid interface formation and its association with battery performance.

Characterizing the distribution of S in the host materials is essential to evaluate the homogeneity of S/host composites

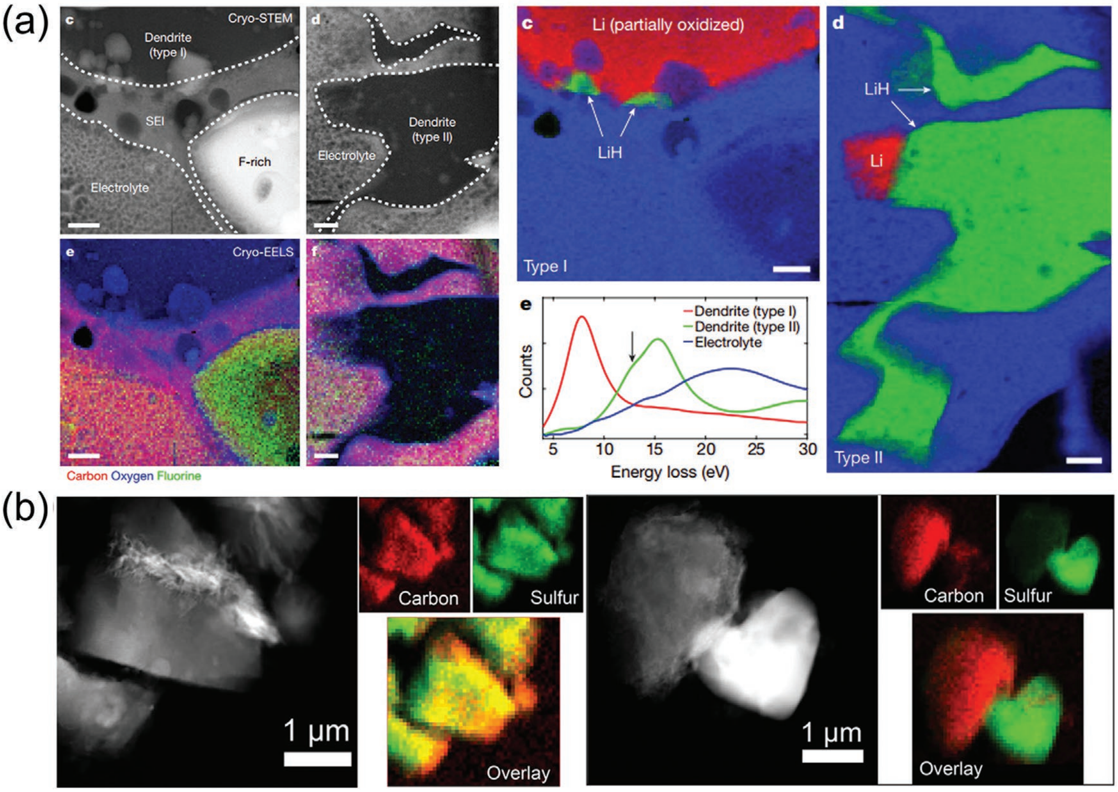

Figure 9. a) Cryo-STEM images and the corresponding EELS elemental mappings, low-loss EELS spectra of the two different types of dendrites. Reproduced with permission.[28a] Copyright 2019, Springer Nature. b) Cryo-STEM images showing the elemental distribution between activated porous carbon with S and nonactivated porous carbons with S. Reproduced with permission.[59] Copyright 2017, Cambridge University Press.

owing to its effect on the performance of Li–S batteries.[56] Designing appropriate composites coupling host materials with uniformly distributed S and detecting their hybrid patterns under microscopically are important.[57] However, S is inclined to sublimate under the high vacuum conditions of an electron microscope sample chamber, resulting in the loss of S from the composite cathode or the redistribution of S within a composite cathode.[58] Additionally, the sublimation of S in the vacuum chamber can pollute the electron microscope and reduce its service life. By contrast, cryo-EM can authentically characterize the distribution of S in the composites by suppressing the sublimation of S and further avoid the potential damages of electron microscopy. Recently, Levin and co-workers enabled the reliable distribution of S in various types of carbon/S composites through cryo-STEM and demonstrated that uniform S infiltration and dispersion through the melt infusion method was easier in activated porous carbon hosts than in nonactivated porous carbon, hollow carbon spheres, and carbon nanotubes (Figure 9b).[59]

The introduction of cryo-STEM for reliable characterizations of sulfur distribution in different host materials provides valuable insights into the design of advanced cathodes in Li–S batteries. However, hitherto, the atomic details and structure changes of S and intermediate polysulfides during charge and discharge processes have not been visualized by cryo-EM. Further visualization of the chemical and structure information at the nanoscale should be performed.

5. Microstructural Characterization by Cryo-FIB

Cryo-TEM can provide high-resolution images and insights into the composition and structure of the SEI and the structure of deposited Li at the nanoscale. However, samples used in cryo-TEM must be extremely thin (<100 nm). Complicated pretreatment processes for traditional bulk materials or cycled bulk Li metals are required. Cryo-FIB has been further developed to characterize air- and heat-sensitive energy materials, especially their cross sections after Ga ion milling at submicron or micron scales.[60] Coupled with EDX analysis, the chemical composition and element content of target samples can be obtained. Compared with standard FIB or SEM, cryo-FIB can more accurately capture the pristine structure and chemical distribution of energy materials. Recently, Meng and co-workers visualized contrasting cross-sectional images of bulk Li metal after milling treatments at cryogenic and room temperatures (**Figure 10**a).[61] Bulk Li metal is likely to undergo local evaporation at room temperature and high vacuum conditions (10^{-6} mbar), in which a network of SEI shell, twisty Li metal, and mossy Li are retained. By contrast, a dense and uniform morphology of bulk Li can be preserved in the pristine state after the milling processes performed using cryo-FIB.

The correlation between battery performance and interface structure is an important factor, as stated above. Archer and coworkers designed a solid–solid interface with fast ion transport by depositing an electrochemically active metal (such as Sn,

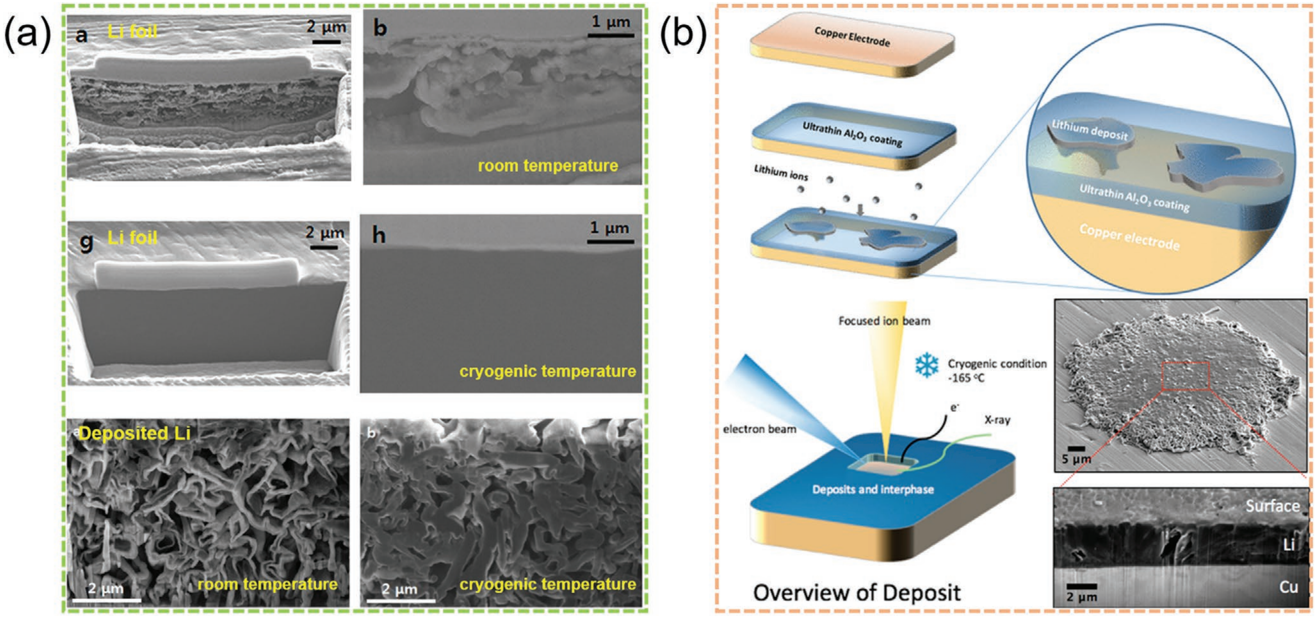

Figure 10. a) Cryo-FIB images of the cross-section of commercial Li foil and deposited Li after milling treatment at room and cryogenic temperature. Reproduced with permission.[61] Copyright 2019, American Chemical Society. b) Schematic illustrations of the ultrathin oxide (Al_2O_3) artificial SEI on conductive substrate and the cross-sectional image of Al_2O_3-coated interphase. Reproduced with permission.[63] Copyright 2018, American Chemical Society.

In, or Si) on a reactive alkali metal electrode.[62] Cryo-FIB was employed to capture the surface and cross-sectional morphology of deposited Li and interfacial compositions were analyzed simultaneously. The captured special multilayer SEI structure included a frozen electrolyte in the top layer, tin-rich middle layer, and bottom Li metal layer. The Sn–Li anode revealed a uniform distribution of Sn nanoparticles on the surface of Li without any Li dendrite formation, which enables a high exchange of current density and stable long-term performance. Archer and co-workers designed a ceramic protective interface (Al_2O_3) for Li metal, exhibiting oxidative stability in both protonic and aprotic liquid electrolytes.[63] Cryo-FIB images revealed that the Al_2O_3 layer served as an effective artificial SEI in a poor SEI-forming propylene carbonate electrolyte (Figure 10b). The compact deposited Li anchored by the ceramic interphase was the source of enhanced stability of Li deposition and high CE of operating batteries.

6. Summary and Outlook

Cryo-EM provides an opportunity for analyzing energy materials precisely by avoiding potential disturbance from air or electron beams. A pristine sample free of contamination or damage can be successfully maintained, and the intrinsic information is available owing to the special sample preparation methods and characterization conditions at cryogenic temperatures of electron microscopy. In addition, cryo-TEM, STEM, and FIB are effective for acquiring multiscale and complementary information of energy materials. Benefiting from the three main techniques developed, the growth behaviors of Li metal, the structure and components of SEIs on electrodes, and the distribution of S in the hosts were characterized closer to reality. Therefore, cryo-EM is a powerful tool for investigating the relation between the operating and failure mechanisms of a battery and the structure and components of electrodes, interfaces, and even electrolytes. Nonetheless, further studies are necessitated to provide a comprehensive and in-depth understanding of energy materials by cryo-EM (**Figure 11**).

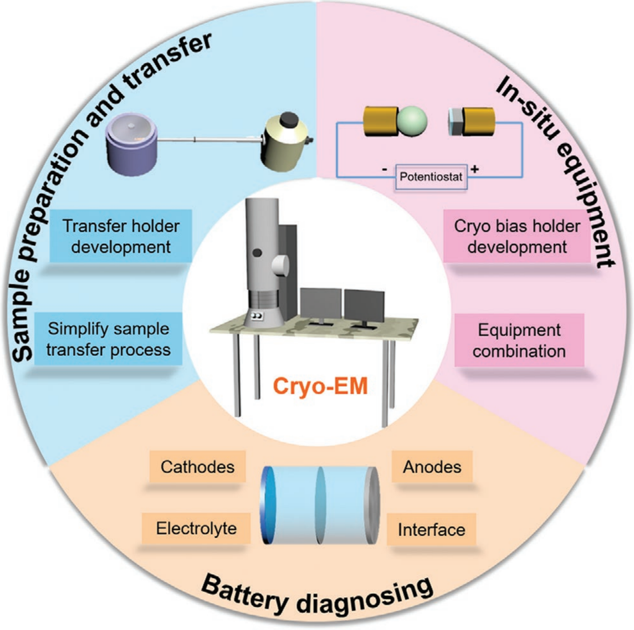

Figure 11. Prospects for the future researches of cryo-EM in the field of secondary battery.

1) Sample preparation and transfer. The sample preparation and transfer processes without specimen destruction and contamination are key to capture the intrinsic information of energy materials. The processes are crucial for cryo-TEM owing to the difficult manipulation of energy materials in a thin size with intrinsically air-sensitive features. Currently, the developed in situ preparation method involves the deposition of Li metal on a TEM grid in a cell and then transferred by a cryo or cooling holder to cryo-TEM, which is an effective method to demonstrate the growth behaviors of Li as well as the components and structure of the SEI. However, the different structures between a TEM grid (Cu-based microgrid or lacey carbon grid) and a Cu current collector in a cell, such as the surface uniformity, can modulate the local current density and the distribution of electric field and ionic concentration, subsequently interfering the formation of deposited Li and SEI on a grid. Therefore, the consistency of Li deposition and the SEI between a grid and a planar Cu current collector or Li foil is the precondition for cryo-TEM characterization. Moreover, the generality of the selected area should be emphasized because the horizon in a cryo-TEM is only confined to the hole of a grid. When FIB is used to mill a sample for the characterization of bulk energy materials at the nanoscale, an advanced inert gas protection device for the fresh milled slice should be introduced to avoid a direct contact of the slice with air during the transfer from cryo-FIB to cryo-TEM. Furthermore, the effects of liquid N_2 at cryogenic temperatures on the structure of Li deposition as well as the components and structure of SEI should be considered. The current preparation and transfer processes for cryo-TEM can be further investigated and modified to accurately provide the pristine features of energy materials and further simplify the operation processes.
2) In situ equipment. In situ observations based on a cryo bias holder in cryo-TEM can dynamically capture the nucleation and growth of Li, the formation of the SEI, and the structure changes of other electrode materials.[64] The in situ detection of the intercalation process of Li ions into a graphite anode, the formation of the SEI, and Li precipitation on graphite provide opportunities to enhance the performance and safety of commercial Li-ion batteries. Advances in TEM in terms of resolution significantly benefit in situ characterizations. By combining with high-resolution three-dimensional reconstruction techniques, the spatial distribution of components in SEIs and electrode materials can be visualized. Additionally, developing cryo-TEM coupled with a spectrometer can yield the real-time structure evolution of energy materials and synchronous regional component analysis during operando experiments. Combining a cryogenic transmission electron microscope with an atomic force microscope cantilever or in situ mechanical testing equipment will be necessary in the future to characterize the mechanical properties of deposited Li and SEIs to deepen the understanding of the growth behavior of Li dendrites and its relation with SEI properties. However, the cryogenic temperature is a significant challenge for the operation of typical instruments.
3) Interfaces. The interface is where electrochemical reactions occur in a battery, which dictates the operating and failure mechanisms of a battery significantly. The formation of an SEI (i.e., the interface between an anode and electrolyte) on a Li metal or other anode materials depends on the operation conditions of a battery. The roles of the types and amounts of solvents, Li salts, and additives, as well as temperature, current density, pressure, and voltage in the components and structure of the SEI can be disclosed by cryo-EM. Moreover, the dynamic changes of an SEI upon cell operations must be fully understood. The CEI on a cathode also exists similarity. Furthermore, the crosstalk of dissolved species between an anode and cathode in a battery is an emerging topic in present and next-generation batteries. For instance, the evolution of structure and composition of the SEI and CEI induced by the dissolution and shuttle effects of polysulfides in the S cathode or transition metal ions in the oxide cathode is garnering increasing attention.
4) Cathodes. The structure change in the surface and bulk of the oxide cathode has been realized by routine electron microscopy. However, the potential effects of air and electron beams on the structure change remain vague. The pristine structure of the surface and bulk of the oxide cathode identified by cryo-EM verified the previous conclusions. Li–S battery is a promising next-generation battery. The conversion mechanism of the S cathode during cycling is still ambiguous owing to the difficult detection of charge and discharge products and intermediates, such as polysulfides, which hinders the rational design of the S cathode severely. Cryo-EM is expected to contribute to the identification of partial intermediates and the corresponding distribution, which will result in a clear scenario related to the conversion of the S cathode.
5) Anodes. The unstable intermediates of anodes in Li-ion and other batteries during charging and discharging processes, such as LiC_x and Li_xSi, can be confirmed at cryogenic conditions. The changes in volume and morphology of the anode after cycling can be more accurately captured by cryo-EM owing to the reduced interference from sample melting by electron beam irradiation at cryogenic temperatures. Moreover, the nucleation, growth, and stripping of Li deposition can be recorded and compared in different electrolytes, current densities, temperatures, and pressures to provide a thorough understanding of the Li metal electrochemistry.
6) Electrolyte. The solvation of Li ions significantly affected the performance of Li metal battery. Limited by the present resolution and precision of cryo-EM, it is difficult to clearly capture the complex solvation structure of Li ions or other alkali metal ions. Owing to the rapid development of cryo-EM techniques, these issues will be disclosed in the future. Additionally, the adsorption form of solvated Li ions on the electrode surface, especially on the SEI and different crystal planes of Li metal, as well as the desolvation pattern of Li ions can be potentially characterized by advanced cryo-EM.

In summary, many successful applications with respect to cryo-EM have been employed to analyze energy materials, which could overcome the vestigial key problems pertaining to batteries. Cryo-EM is a powerful tool for investigating the relationship between the operating and failure mechanisms of batteries as well as the structure and components of electrodes, interfaces, and even electrolytes by preserving the pristine state of air- and beam-sensitive energy materials. With the assistance of cryo-TEM, novel discoveries in battery studies are emerging, which challenge traditional approaches. Cryo-EM will continuously provide new perspectives for battery studies and guide the rational design of energy materials for a sustainable society.

Acknowledgements

This work was supported by National Key Research and Development Program (2016YFA0202500), National Natural Science Foundation of China (21825501 and U1801257), Beijing Natural Science Foundation (L182021), and Tsinghua University Initiative Scientific Research Program.

Conflict of Interest

The authors declare no conflict of interest.

Keywords

cryogenic electron microscopy, electrolytes, lithium metal anodes, rechargeable batteries, solid electrolytes interphases

Received: December 18, 2019
Revised: February 27, 2020

[1] a) J. M. Tarascon, M. Armand, *Nature* **2001**, *414*, 359; b) H. Zhang, C. Li, G. G. Eshetu, S. Laruelle, S. Grugeon, K. Zaghib, C. Julien, A. Mauger, D. Guyomard, T. Rojo, N. Gisbert-Trejo, S. Passerini, X. Huang, Z. Zhou, P. Johansson, M. Forsyth, *Angew. Chem., Int. Ed.* **2020**, *59*, 534; c) M. Li, J. Lu, Z. Chen, K. Amine, *Adv. Mater.* **2018**, *30*, 1800561.

[2] a) M. Armand, J. M. Tarascon, *Nature* **2008**, *451*, 652; b) J. Liu, Z. Bao, Y. Cui, E. J. Dufek, J. B. Goodenough, P. Khalifah, Q. Li, B. Y. Liaw, P. Liu, A. Manthiram, Y. S. Meng, V. R. Subramanian, M. F. Toney, V. V. Viswanathan, M. S. Whittingham, J. Xiao, W. Xu, J. Yang, X.-Q. Yang, J.-G. Zhang, *Nat. Energy* **2019**, *4*, 180; c) H. Duan, M. Fan, W.-P. Chen, J.-Y. Li, P.-F. Wang, W.-P. Wang, J.-L. Shi, Y.-X. Yin, L.-J. Wan, Y.-G. Guo, *Adv. Mater.* **2019**, *31*, 1807789.

[3] a) S. Chu, Y. Cui, N. Liu, *Nat. Mater.* **2017**, *16*, 16; b) C. Z. Zhao, H. Duan, J.-Q. Huang, J. Zhang, Q. Zhang, Y.-G. Guo, L.-J. Wan, *Sci. China: Chem.* **2019**, *62*, 1286; c) Y. Liang, C.-Z. Zhao, H. Yuan, Y. Chen, W. Zhang, J.-Q. Huang, D. Yu, Y. Liu, M.-M. Titirici, Y.-L. Chueh, H. Yu, Q. Zhang, *InfoMat* **2019**, *1*, 6; d) L. Jiang, X.-B. Cheng, H.-J. Peng, J.-Q. Huang, Q. Zhang, *eTransportation* **2019**, *2*, 100033.

[4] a) D. Bresser, K. Hosoi, D. Howell, H. Li, H. Zeisel, K. Amine, S. Passerini, *J. Power Sources* **2018**, *382*, 176; b) Y. X. Lu, X. H. Rong, Y. S. Hu, L. Q. Chen, H. Li, *Energy Storage Mater.* **2019**, *23*, 144; c) X. Q. Zhang, C. Z. Zhao, J. Q. Huang, Q. Zhang, *Engineering* **2018**, *4*, 831; d) X. Ren, Z. Ren, Q. Li, W. Wen, X. Li, Y. Chen, L. Xie, L. Zhang, D. Zhu, B. Gao, P. K. Chu, K. Huo, *Adv. Energy Mater.* **2019**, *9*, 1900091.

[5] a) T. Placke, R. Kloepsch, S. Dühnen, M. Winter, *J. Solid State Electrochem.* **2017**, *21*, 1939; b) R. Schmuch, R. Wagner, G. Horpel, T. Placke, M. Winter, *Nat. Energy* **2018**, *3*, 267; c) J. Betz, J.-P. Brinkmann, R. Noelle, C. Luerenbaum, M. Kolek, M. C. Stan, M. Winter, T. Placke, *Adv. Energy Mater.* **2019**, *9*, 1900574.

[6] a) X. Wang, Y. Li, Y. S. Meng, *Joule* **2018**, *2*, 2225; b) E. J. Berg, C. Villevieille, D. Streich, S. Trabesinger, P. Novak, *J. Electrochem. Soc.* **2015**, *162*, A2468; c) H. Liu, X.-B. Cheng, Z. Jin, R. Zhang, G. Wang, L.-Q. Chen, Q.-B. Liu, J.-Q. Huang, Q. Zhang, *EnergyChem* **2019**, *1*, 100003; d) X.-B. Cheng, C.-Z. Zhao, Y.-X. Yao, H. Liu, Q. Zhang, *Chem* **2019**, *5*, 74.

[7] a) X. B. Cheng, R. Zhang, C. Z. Zhao, Q. Zhang, *Chem. Rev.* **2017**, *117*, 10403; b) L. Wang, Z. Zhou, X. Yan, F. Hou, L. Wen, W. Luo, J. Liang, S. X. Dou, *Energy Storage Mater.* **2018**, *14*, 22; c) D. Lin, Y. Liu, Y. Cui, *Nat. Nanotechnol.* **2017**, *12*, 194; d) Y. Ma, S. Li, B. Wei, *Nanoscale* **2019**, *11*, 20429.

[8] a) X. Ji, *Energy Environ. Sci.* **2019**, *12*, 3203; b) W. Xu, J. L. Wang, F. Ding, X. L. Chen, E. Nasybutin, Y. H. Zhang, J. G. Zhang, *Energy Environ. Sci.* **2014**, *7*, 513; c) Y.-S. Hong, C.-Z. Zhao, Y. Xiao, R. Xu, J.-J. Xu, J.-Q. Huang, Q. Zhang, X. Yu, H. Li, *Batteries Supercaps* **2019**, *2*, 638.

[9] a) Y. Li, Y. Li, Y. Sun, B. Butz, K. Yan, A. L. Koh, J. Zhao, A. Pei, Y. Cui, *Nano Lett.* **2017**, *17*, 5171; b) H. Ye, C.-Y. Wang, T.-T. Zuo, P.-F. Wang, Y.-X. Yin, Z.-J. Zheng, P. Wang, J. Cheng, F.-F. Cao, Y.-G. Guo, *Nano Energy* **2018**, *48*, 369; c) D. Liu, Z. Shadike, R. Lin, K. Qian, H. Li, K. Li, S. Wang, Q. Yu, M. Liu, S. Ganapathy, X. Qin, Q.-H. Yang, M. Wagemaker, F. Kang, X.-Q. Yang, B. Li, *Adv. Mater.* **2019**, *31*, 1806620.

[10] a) X. Q. Zhang, X. B. Cheng, Q. Zhang, *Adv. Mater. Interfaces* **2018**, *5*, 1701097; b) X.-Q. Zhang, X.-B. Cheng, X. Chen, C. Yan, Q. Zhang, *Adv. Funct. Mater.* **2017**, *27*, 1605989; c) X. Shen, X. Cheng, P. Shi, J. Huang, X. Zhang, C. Yan, T. Li, Q. Zhang, *J. Energy Chem.* **2019**, *37*, 29; d) Z. Ju, J. Nai, Y. Wang, T. Liu, J. Zheng, H. Yuan, O. Sheng, C. Jin, W. Zhang, Z. Jin, H. Tian, Y. Liu, X. Tao, *Nat. Commun.* **2020**, *11*, 488; e) B. Q. Li, L. Kong, C. X. Zhao, Q. Jin, X. Chen, H. J. Peng, J. L. Qin, J. X. Chen, H. Yuan, Q. Zhang, J. Q. Huang, *InfoMat* **2019**, *1*, 533.

[11] B. J. Neudecker, N. J. Dudney, J. B. Bates, *J. Electrochem. Soc.* **2000**, *147*, 517.

[12] Y. Li, Y. Li, A. Pei, K. Yan, Y. Sun, C.-L. Wu, L.-M. Joubert, R. Chin, A. L. Koh, Y. Yu, J. Perrino, B. Butz, S. Chu, Y. Cui, *Science* **2017**, *358*, 506.

[13] a) K. Xu, *Chem. Rev.* **2004**, *104*, 4303; b) X. B. Cheng, R. Zhang, C. Z. Zhao, F. Wei, J. G. Zhang, Q. Zhang, *Adv. Sci.* **2016**, *3*, 1500213; c) Y. Yuan, F. Wu, G. Chen, Y. Bai, C. Wu, *J. Energy Chem.* **2019**, *37*, 197; d) Y. Fan, T. Wang, D. Legut, Q. Zhang, *J. Energy Chem.* **2019**, *39*, 160.

[14] a) P. Verma, P. Maire, P. Novak, *Electrochim. Acta* **2010**, *55*, 6332; b) S. Komaba, W. Murata, T. Ishikawa, N. Yabuuchi, T. Ozeki, T. Nakayama, A. Ogata, K. Gotoh, K. Fujiwara, *Adv. Funct. Mater.* **2011**, *21*, 3859; c) M. D. Tikekar, S. Choudhury, Z. Y. Tu, L. A. Archer, *Nat. Energy* **2016**, *1*, 16114; d) E. Markevich, G. Salitra, F. Chesneau, M. Schmidt, D. Aurbach, *ACS Energy Lett.* **2017**, *2*, 1321.

[15] a) E. Peled, S. Menkin, *J. Electrochem. Soc.* **2017**, *164*, A1703; b) K. Xu, *Chem. Rev.* **2014**, *114*, 11503; c) B. Q. Li, X. R. Chen, X. Chen, C. X. Zhao, R. Zhang, X. B. Cheng, Q. Zhang, *Research* **2019**, *2019*, 4608940.

[16] a) D. Aurbach, *J. Power Sources* **2000**, *89*, 206; b) D. Aurbach, Y. Talyosef, B. Markovsky, E. Markevich, E. Zinigrad, L. Asraf, J. S. Gnanaraj, H. J. Kim, *Electrochim. Acta* **2004**, *50*, 247; c) T. Li, X.-Q. Zhang, P. Shi, Q. Zhang, *Joule* **2019**, *3*, 2647; d) X. W. Yu, A. Manthiram, *Energy Environ. Sci.* **2018**, *11*, 527; e) M. Gauthier, T. J. Carney, A. Grimaud, L. Giordano, N. Pour, H.-H. Chang, D. P. Fenning, S. F. Lux, O. Paschos, C. Bauer, F. Maglia, S. Lupart, P. Lamp, Y. Shao-Horn, *J. Phys. Chem. Lett.* **2015**, *6*, 4653.

[17] a) Y. Qian, P. Niehoff, M. Boerner, M. Gruetzke, X. Moennighoff, P. Behrends, S. Nowak, M. Winter, F. M. Schappacher, *J. Power Sources* **2016**, *329*, 31; b) J.-N. Zhang, Q. Li, Y. Wang, J. Zheng, X. Yu, H. Li, *Energy Storage Mater.* **2018**, *14*, 1.

[18] K. A. Taylor, R. M. Glaeser, *Science* **1974**, *186*, 1036.

[19] a) Y. Chen, L. Zheng, D. C. Johnson, C. L. Campion, *Chem* **2018**, *4*, 2254; b) W. J. E. M. Habraken, J. Tao, L. J. Brylka, H. Friedrich, L. Bertinetti, A. S. Schenk, A. Verch, V. Dmitrovic, P. H. H. Bomans, P. M. Frederik, J. Laven, P. van der Schoot, B. Aichmayer, G. de With, J. J. DeYoreo, N. A. J. M. Sommerdijk, *Nat. Commun.* **2013**, *4*, 1507.

[20] a) W. Zhang, Z. Kochovski, Y. Lu, B. V. K. J. Schmidt, M. Antonietti, J. Yuan, *ACS Nano* **2016**, *10*, 7731; b) M. R. Dreher, A. J. Simnick, K. Fischer, R. J. Smith, A. Patel, M. Schmidt, A. Chilkoti, *J. Am. Chem. Soc.* **2008**, *130*, 687.

[21] a) S. Mornet, O. Lambert, E. Duguet, A. Brisson, *Nano Lett.* **2005**, *5*, 281; b) Y. Li, K. Wang, W. Zhou, Y. Li, R. Vila, W. Huang, H. Wang, G. Chen, G.-H. Wu, Y. Tsao, H. Wang, R. Sinclair, W. Chiu, Y. Cui, *Matter* **2019**, *1*, 428.

[22] a) X. Wang, M. Zhang, J. Alvarado, S. Wang, M. Sina, B. Lu, J. Bouwer, W. Xu, J. Xiao, J.-G. Zhang, J. Liu, Y. S. Meng, *Nano Lett.* **2017**, *17*, 7606; b) Y. Yang, D. M. Davies, Y. Yin, O. Borodin, J. Z. Lee, C. Fang, M. Olguin, Y. Zhang, E. S. Sablina, X. Wang, C. S. Rustomji, Y. S. Meng, *Joule* **2019**, *3*, 1986.

[23] a) Y. Yuan, J. Lu, *Chem* **2018**, *4*, 2253; b) K. Yan, J. Wang, S. Zhao, D. Zhou, B. Sun, Y. Cui, G. Wang, *Angew. Chem., Int. Ed.* **2019**, *58*, 11364; c) S.-H. Yu, M. J. Zachman, K. Kang, H. Gao, X. Huang, F. J. DiSalvo, J. Park, L. F. Kourkoutis, H. D. Abruña, *Adv. Energy Mater.* **2019**, *9*, 1902773.

[24] a) M. J. Zachman, N. de Jonge, R. Fischer, K. L. Jungjohann, D. E. Perea, *MRS Bull.* **2019**, *44*, 949; b) C. Zhang, Y. Feng, Z. Han, S. Gao, M. Wang, P. Wang, *Adv. Mater.* **2019**, *31*, 1903747.

[25] a) N. I. Kato, *J. Electron Microsc.* **2004**, *53*, 451; b) A. Rigort, J. M. Plitzko, *Arch. Biochem. Biophys.* **2015**, *581*, 122.

[26] A. Bartesaghi, A. Merk, S. Banerjee, D. Matthies, X. Wu, J. L. S. Milne, S. Subramaniam, *Science* **2015**, *348*, 1147.

[27] M. J. Zachman, E. Asenath-Smith, L. A. Estroff, L. F. Kourkoutis, *Microsc. Microanal.* **2016**, *22*, 1338.

[28] a) M. J. Zachman, Z. Tu, S. Choudhury, L. A. Archer, L. F. Kourkoutis, *Nature* **2018**, *560*, 345; b) Z. Tu, S. Choudhury, M. J. Zachman, S. Wei, K. Zhang, L. F. Kourkoutis, L. A. Archer, *Joule* **2017**, *1*, 394.

[29] W. Huang, J. Wang, M. R. Braun, Z. Zhang, Y. Li, D. T. Boyle, P. C. McIntyre, Y. Cui, *Matter* **2019**, *1*, 1232.

[30] H. Liu, X. Wang, H. Zhou, H.-D. Lim, X. Xing, Q. Yan, Y. S. Meng, P. Liu, *ACS Appl. Energy Mater.* **2018**, *1*, 1864.

[31] a) X. H. Liu, J. W. Wang, S. Huang, F. Fan, X. Huang, Y. Liu, S. Krylyuk, J. Yoo, S. A. Dayeh, A. V. Davydov, S. X. Mao, S. T. Picraux, S. Zhang, J. Li, T. Zhu, J. Y. Huang, *Nat. Nanotechnol.* **2012**, *7*, 749; b) J. Y. Huang, L. Zhong, C. M. Wang, J. P. Sullivan, W. Xu, L. Q. Zhang, S. X. Mao, N. S. Hudak, X. H. Liu, A. Subramanian, H. Fan, L. Qi, A. Kushima, J. Li, *Science* **2010**, *330*, 1515; c) X. Ren, J. Wang, D. Zhu, Q. Li, W. Tian, L. Wang, J. Zhang, L. Miao, P. K. Chu, K. Huo, *Nano Energy* **2018**, *54*, 322; d) C. Zhang, K. L. Firestein, J. F. S. Fernando, D. Siriwardena, J. E. von Treifeldt, D. Golberg, *Adv. Mater.* **2020**, *32*, 1904094.

[32] M. M. Markowitz, D. A. Boryta, *J. Chem. Eng. Data* **1962**, *7*, 586.

[33] R. F. Egerton, P. Li, M. Malac, *Micron* **2004**, *35*, 399.

[34] K. W. Urban, *Science* **2008**, *321*, 506.

[35] a) A. Kushima, K. P. So, C. Su, P. Bai, N. Kuriyama, T. Maebashi, Y. Fujiwara, M. Z. Bazant, J. Li, *Nano Energy* **2017**, *32*, 271; b) R. Xu, X.-B. Cheng, C. Yan, X.-Q. Zhang, Y. Xiao, C.-Z. Zhao, J.-Q. Huang, Q. Zhang, *Matter* **2019**, *1*, 317.

[36] a) C. Yan, H.-R. Li, X. Chen, X.-Q. Zhang, X.-B. Cheng, R. Xu, J.-Q. Huang, Q. Zhang, *J. Am. Chem. Soc.* **2019**, *141*, 9422; b) X. Fan, X. Ji, L. Chen, J. Chen, T. Deng, F. Han, J. Yue, N. Piao, R. Wang, X. Zhou, X. Xiao, L. Chen, C. Wang, *Nat. Energy* **2019**, *4*, 882; c) Y. Xu, H. Wu, Y. He, Q. Chen, J. G. Zhang, W. Xu, C. Wang, *Nano Lett.* **2020**, *20*, 418; d) A. C. Thenuwara, P. P. Shetty, M. T. McDowell, *Nano Lett.* **2019**, *19*, 8664.

[37] C. Hou, J. Han, P. Liu, C. Yang, G. Huang, T. Fujita, A. Hirata, M. Chen, *Adv. Energy Mater.* **2019**, *9*, 1902675.

[38] a) S. S. Zhang, *J. Power Sources* **2006**, *162*, 1379; b) R. Mogi, M. Inaba, S. K. Jeong, Y. Iriyama, T. Abe, Z. Ogumi, *J. Electrochem. Soc.* **2002**, *149*, A1578; c) C. Yan, X. B. Cheng, Y. Tian, X. Chen, X. Q. Zhang, W. J. Li, J. Q. Huang, Q. Zhang, *Adv. Mater.* **2018**, *30*, 1707629.

[39] E. Peled, D. Golodnitsky, G. Ardel, *J. Electrochem. Soc.* **1997**, *144*, L208.

[40] D. Aurbach, Y. Einely, A. Zaban, *J. Electrochem. Soc.* **1994**, *141*, L1.

[41] Y. Liu, D. Lin, Y. Li, G. Chen, A. Pei, O. Nix, Y. Li, Y. Cui, *Nat. Commun.* **2018**, *9*, 3656.

[42] J. Wang, W. Huang, A. Pei, Y. Li, F. Shi, X. Yu, Y. Cui, *Nat. Energy* **2019**, *4*, 664.

[43] H. Wang, Y. Li, Y. Li, Y. Liu, D. Lin, C. Zhu, G. Chen, A. Yang, K. Yan, H. Chen, Y. Zhu, J. Li, J. Xie, J. Xu, Z. Zhang, R. Vila, A. Pei, K. Wang, Y. Cui, *Nano Lett.* **2019**, *19*, 1326.

[44] N. Sata, K. Eberman, K. Eberl, J. Maier, *Nature* **2000**, *408*, 946.

[45] a) W. Wieczorek, K. Such, H. Wycislik, J. Plocharski, *Solid State Ionics* **1989**, *36*, 255; b) W. Wieczorek, Z. Florjanczyk, J. R. Stevens, *Electrochim. Acta* **1995**, *40*, 2251.

[46] Y. Li, W. Huang, Y. Li, A. Pei, D. T. Boyle, Y. Cui, *Joule* **2018**, *2*, 2167.

[47] C. Fang, J. Li, M. Zhang, Y. Zhang, F. Yang, J. Z. Lee, M.-H. Lee, J. Alvarado, M. A. Schroeder, Y. Yang, B. Lu, N. Williams, M. Ceja, L. Yang, M. Cai, J. Gu, K. Xu, X. Wang, Y. S. Meng, *Nature* **2019**, *572*, 511.

[48] W. Huang, P. M. Attia, H. S. Wang, S. E. Renfrew, N. Jin, S. Das, Z. W. Zhang, D. T. Boyle, Y. Z. Li, M. Z. Bazant, B. D. McCloskey, W. C. Chueh, Y. Cui, *Nano Lett.* **2019**, *19*, 5140.

[49] Y. C. Chen, C. Y. Ouyang, L. J. Song, Z. L. Sun, *J. Phys. Chem. C* **2011**, *115*, 7044.

[50] W. Huang, D. T. Boyle, Y. Li, Y. Li, A. Pei, H. Chen, Y. Cui, *ACS Nano* **2019**, *13*, 737.

[51] a) D. Lin, Y. Liu, W. Chen, G. Zhou, K. Liu, B. Dunn, Y. Cui, *Nano Lett.* **2017**, *17*, 3731; b) N.-W. Li, Y.-X. Yin, C.-P. Yang, Y.-G. Guo, *Adv. Mater.* **2016**, *28*, 1853; c) H.-D. Lim, H.-K. Lim, X. Xing, B.-S. Lee, H. Liu, C. Coaty, H. Kim, P. Liu, *Adv. Mater. Interfaces* **2018**, *5*, 1701328; d) R. Xu, Y. Xiao, R. Zhang, X.-B. Cheng, C.-Z. Zhao, X.-Q. Zhang, C. Yan, Q. Zhang, J.-Q. Huang, *Adv. Mater.* **2019**, *31*, 1808392.

[52] Y. Gao, Z. Yan, J. L. Gray, X. He, D. Wang, T. Chen, Q. Huang, Y. C. Li, H. Wang, S. H. Kim, T. E. Mallouk, D. Wang, *Nat. Mater.* **2019**, *18*, 384.

[53] J. Alvarado, M. A. Schroeder, M. Zhang, O. Borodin, E. Gobrogge, M. Olguin, M. S. Ding, M. Gobet, S. Greenbaum, Y. S. Meng, K. Xu, *Mater. Today* **2018**, *21*, 341.

[54] X. Xing, Y. Li, X. Wang, V. Petrova, H. Liu, P. Liu, *Energy Storage Mater.* **2019**, *21*, 474.

[55] S. J. Pennycook, L. A. Boatner, *Nature* **1988**, *336*, 565.

[56] a) J. Zhang, Z. Li, Y. Chen, S. Gao, X. W. Lou, *Angew. Chem., Int. Ed.* **2018**, *57*, 10944; b) H. Jiang, X.-C. Liu, Y. Wu, Y. Shu, X. Gong, F.-S. Ke, H. Deng, *Angew. Chem., Int. Ed.* **2018**, *57*, 3916; c) H. Yuan, H.-J. Peng, J.-Q. Huang, Q. Zhang, *Adv. Mater. Interfaces* **2019**, *6*, 1802046.

[57] a) S. D. Talian, G. Kapun, J. Moskon, A. Vizintin, A. Randon-Vitanova, R. Dominko, M. Gaberscek, *Chem. Mater.* **2019**, *31*, 9012; b) N. Zhang, B. D. A. Levin, Y. Yang, D. A. Muller, H. D. Abruna, *J. Electrochem. Soc.* **2018**, *165*, A1656; c) X.-C. Liu, Y. Yang, J. Wu, M. Liu, S. P. Zhou, B. D. A. Levi, X.-D. Zhou, H. Cong, D. A. Muller, P. M. Ajayan, H. D. Abruna, F.-S. Ke, *ACS Energy Lett.* **2018**, *3*, 1325.

[58] a) C. Raiss, K. Peppler, J. Janek, P. Adelhelm, *Carbon* **2014**, *79*, 245; b) A. G. M. Ferreira, L. Q. Lobo, *J. Chem. Thermodyn.* **2011**, *43*, 95.

[59] B. D. A. Levin, M. J. Zachman, J. G. Werner, R. Sahore, K. X. Nguyen, Y. Han, B. Xie, L. Ma, L. A. Archer, E. P. Giannelis, U. Wiesner, L. F. Kourkoutis, D. A. Muller, *Microsc. Microanal.* **2017**, *23*, 155.
[60] S. Lim, S. Kim, K. H. Ahn, S. J. Lee, *J. Power Sources* **2015**, *299*, 221.
[61] J. Z. Lee, T. A. Wynn, M. A. Schroeder, J. Alvarado, X. Wang, K. Xu, Y. S. Meng, *ACS Energy Lett.* **2019**, *4*, 489.
[62] Z. Tu, S. Choudhury, M. J. Zachman, S. Wei, K. Zhang, L. F. Kourkoutis, L. A. Archer, *Nat. Energy* **2018**, *3*, 310.
[63] Z. Tu, M. J. Zachman, S. Choudhury, K. A. Khan, Q. Zhao, L. F. Kourkoutis, L. A. Archer, *Chem. Mater.* **2018**, *30*, 5655.
[64] Z. Fan, L. Zhang, D. Baumann, L. Mei, Y. Yao, X. Duan, Y. Shi, J. Huang, Y. Huang, X. Duan, *Adv. Mater.* **2019**, *31*, 1900608.